

Clean and Hydrogen-Adsorbed AlInP(001) Surfaces: Structures and Electronic Properties

Luis Joel Glahn, Isaac Azahel Ruiz Alvarado,* Sergej Neufeld, Mohammad Amin Zare Pour, Agnieszka Paszuk, David Ostheimer, Sahar Shekarabi, Oleksandr Romanyuk, Dominik Christian Moritz, Jan Philipp Hofmann, Wolfram Jaegermann, Thomas Hannappel, and Wolf Gero Schmidt

Total energy and electronic structure calculations based on density functional theory are performed in order to determine the atomic structure and electronic properties of clean and hydrogen-adsorbed $\text{Al}_{0.5}\text{In}_{0.5}\text{P}(001)$ surfaces. It is found that most of the stable surfaces obey the electron-counting rule and are characterized by surface atom dimerization. The dimer-related surface states are predicted to occur in the vicinity of the bulk band edges. For a very narrow range of preparation conditions, ab initio thermodynamics predicts metal atomic wires formed by surface cations. A surface covered with a monolayer of buckled phosphorus dimers, where half of the phosphorus atoms are hydrogen saturated, is found to be stable for metal–organic vapor-phase epitaxy growth conditions. The occurrence of this structure is confirmed by low-energy electron diffraction and X-ray photoelectron spectroscopy data measured on epitaxially grown $\text{Al}_{0.52}\text{In}_{0.48}\text{P}(001)$ epilayers lattice matched to GaAs.

1. Introduction

III–V compound semiconductors are important for various electronic and optoelectronic applications, for example, high-electron-mobility transistors, light-emitting diodes, photodetectors, electro-optic modulators, and frequency-mixing components. Solar cells made of III–V semiconductors reach the highest efficiencies of any photovoltaic technology so far.^[1] The $\text{Al}_x\text{In}_{1-x}\text{P}$ (AlInP) material system is frequently used as window layer in solar cells, due to its favorable combination of chemical stability, sufficiently wide bandgap, and high-quality heteroepitaxial interfaces with many absorbers.^[2] In this context, the Fermi-level pinning due to AlInP surface states is highly relevant for device performance.^[3] This holds also for the usage of AlInP as intermediate layer to form low-resistance ohmic contacts.^[4]

Previous work on III–V ternary alloys focuses primarily on the structural and electronic properties of the bulk, see, for example, other studies^[5–8] and heterostructure interfaces.^[9–12] There is little information available on the atomic structure and electronic properties of AlInP surfaces. It has been noted that different growth conditions lead to different degrees of CuPt ordering in the bulk material,^[13,14] that is, alternating group III layers perpendicular to the $\bar{1}11$ or $1\bar{1}1$ directions. This is likely to be related to the formation of surface dimers, which induce strain in the material.^[15,16] In case of GaInP, the CuPt-type ordering has been found to cause anisotropic effects in the electrical and optical properties.^[17,18]

Very recently, some models for clean AlInP(001) surfaces were established, which show that structures different from the ones known from binary III–V(001) surfaces may occur.^[19] However, the calculations in the study by Ruiz Alvarado et al.^[19] are restricted to clean surfaces. Often, AlInP is grown by metal–organic vapor-phase epitaxy (MOVPE) and chemical beam epitaxy (CBE). Since hydrogen is present in MOVPE and CBE, it can be expected to be present at the AlInP surface as well.^[20,21] Therefore, we here extend the previous study^[19] to account for the possibility of surface-adsorbed hydrogen.


A systematic search for stable $\text{Al}_{0.5}\text{In}_{0.5}\text{P}(001)$ surface structures is performed, where the existence of hydrogen is

L. J. Glahn, I. A. Ruiz Alvarado, S. Neufeld, W. G. Schmidt
Lehrstuhl für Theoretische Materialphysik
Universität Paderborn
33095 Paderborn, Germany
E-mail: azahel@mail.upb.de

M. A. Zare Pour, A. Paszuk, D. Ostheimer, S. Shekarabi, T. Hannappel
Institut für Physik
Technische Universität Ilmenau
Gustav-Kirchhoff-Strasse 5, 98693 Ilmenau, Germany

O. Romanyuk
Institute of Physics
Academy of Sciences of the Czech Republic
Cukrovarnicka 10, 16200 Prague, Czech Republic

D. C. Moritz, J. P. Hofmann, W. Jaegermann
Surface Science Laboratory
Department of Materials and Earth Sciences
Technische Universität Darmstadt
Otto-Berndt-Strasse 3, 64287 Darmstadt, Germany

 The ORCID identification number(s) for the author(s) of this article can be found under <https://doi.org/10.1002/pssb.202200308>.

© 2022 The Authors. physica status solidi (b) basic solid state physics published by Wiley-VCH GmbH. This is an open access article under the terms of the Creative Commons Attribution License, which permits use, distribution and reproduction in any medium, provided the original work is properly cited.

DOI: 10.1002/pssb.202200308

considered as an additional degree of freedom. The initial geometries for structure optimization are generated by systematically varying the surface stoichiometry of both CuPt–A and CuPt–B-type ordered $\text{Al}_{0.5}\text{In}_{0.5}\text{P}$ crystals. The commonly accepted III–V(001) surface reconstructions^[20–22] are included in the calculations, which probe computationally more than 80 surfaces. The computational predictions for typical MOVPE growth conditions are compared with low-energy electron diffraction (LEED) and X-ray photoelectron spectroscopy (XPS) data measured on epitaxially grown $\text{Al}_{0.52}\text{In}_{0.48}\text{P}$ (001) samples.

2. Computational Methodology

In detail, density functional theory (DFT) calculations are performed using the Vienna ab initio simulation package (VASP).^[23] The generalized gradient approximation (GGA) with the PBE functional^[24] is used to model the electron exchange and correlation interaction. The electron–ion interaction is described by the projector-augmented wave (PAW) scheme.^[25,26] The electronic wave functions are expanded into plane waves up to a kinetic energy cutoff of 400 eV. The (001) surfaces are modeled by supercells containing 13 and 14 atomic layers for cation- and anion-terminated surfaces, respectively, and vacuum regions of $\approx 13.5 \text{ \AA}$. 2×2 , 2×4 , and $c\text{-}4 \times 4$ translational symmetries are considered. The slab bottom dangling bonds are saturated with fractionally charged H atoms. The electric field resulting from the inequivalence of the two surfaces is taken into account by a dipole correction to the electrostatic potential. The atoms are structurally relaxed until they experience forces smaller than 0.02 eV \AA^{-1} . The calculations are performed at the equilibrium lattice parameter of $\text{Al}_{0.5}\text{In}_{0.5}\text{P}$ calculated to be 5.751 \AA . The Brillouin zone integration is performed using a \mathbf{k} -point mesh corresponding to 64 sampling points in the primitive cell.

In order to compare the various clean and hydrogen-covered surfaces energetically, the chemical potentials μ_{A_i} of the respective surface constituents need to be taken into account. The surface ground state is determined by the minimum of the thermodynamic potential

$$\Omega = U - TS - \sum_i \mu_{A_i} n_{A_i} \quad (1)$$

where U is the total energy of the system. In solids, the entropy term, TS , contributes very little to the difference in Ω under usual experimental conditions^[27] and is neglected in the following. The chemical potentials μ_{A_i} for $A_i = \text{In}$, Al , and P are restricted by their bulk values

$$\mu_{A_i} \leq \mu_{A_i,\text{bulk}} \quad (2)$$

In addition, the stability of $\text{Al}_{0.5}\text{In}_{0.5}\text{P}$ requires

$$\begin{aligned} \mu_{\text{Al}} + \mu_{\text{In}} + 2\mu_{\text{P}} &= \mu_{\text{AlInP}_2,\text{bulk}} \\ &= \mu_{\text{Al,bulk}} + \mu_{\text{In,bulk}} + 2\mu_{\text{P,bulk}} \\ &\quad + \Delta H_{f,\text{AlInP}_2} \end{aligned} \quad (3)$$

This allows for formulating the formation energy depending on $\Delta\mu_{\text{In}}$ and $\Delta\mu_{\text{Al}}$, that is, the variations of the In and Al chemical potentials with respect to their bulk values. For the heat of

formation $\Delta H_{f,\text{AlInP}_2}$ we calculate a value of -1.49 eV . The hydrogen chemical potential, $\Delta\mu_{\text{H}}$, with respect to an isolated molecule, provides an additional and independent degree of freedom. In the approximation of a two-atomic ideal gas, it is written depending on partial pressure p and temperature T as

$$\Delta\mu_{\text{H}}(p, T) = \frac{k_{\text{B}}T}{2} \left[\ln \left\{ \frac{p\lambda^3}{k_{\text{B}}T} \right\} - \ln Z_{\text{rot}} - \ln Z_{\text{vib}} \right] \quad (4)$$

where k_{B} is the Boltzmann constant, λ the de Broglie thermal wavelength of the H_2 molecule,

$$\lambda = \sqrt{\frac{2\pi\hbar^2}{mk_{\text{B}}T}} \quad (5)$$

and Z_{rot} and Z_{vib} are its rotational and vibrational partition functions, respectively.

$$Z_{\text{rot}} = \sum_{J=0}^{\infty} (2J+1) \exp\left(\frac{-J(J+1)\hbar}{2Ik_{\text{B}}T}\right) \quad (6)$$

$$Z_{\text{vib}} = \frac{\hbar\omega}{2} + k_{\text{B}}T \ln\left(1 - \exp\left(\frac{\hbar\omega}{k_{\text{B}}T}\right)\right) \quad (7)$$

Here I is the moment of inertia and ω the fundamental mode of H_2 . By increasing the temperature, the hydrogen chemical potential is lowered, that is, less energy is gained by taking a H atom out of the reservoir and attaching it to the surface. A variation of the hydrogen chemical potential with respect to its molecular value at zero temperature of $\Delta\mu_{\text{H}} = -0.6 \text{ eV}$ corresponds to the growth conditions in the experiment described below.

3. Results and Discussion

3.1. Surface Phase Diagram

Figure 1 shows the calculated phase diagram of the $\text{Al}_{0.5}\text{In}_{0.5}\text{P}$ (001) surface structures considered here. Only 10 out of the more than 80 candidate structures considered in our work turn out to be energetically relevant, that is, correspond to the surface ground state for specific preparation conditions. Schematic top views of these surfaces are compiled in Figure 2. The notation of structures, if not known taken from earlier studies, was chosen such as to indicate the translational symmetry, surface stoichiometry, and the presence of dimers (D) and mixed heterodimers (MD) of the respective surface.

At hydrogen-deficient conditions ($\Delta\mu_{\text{H}} = -1 \text{ eV}$), P-dimer structures known from clean III–V(001) surfaces^[22,28] dominate the phase diagram. This concerns the $c\text{-}4 \times 4$ structure for anion-rich surfaces and the $\beta 2\text{-}2 \times 4$ surface for intermediate preparation conditions. The occurrence of [110]-oriented P dimers in the P-rich $c\text{-}4 \times 4$ structure and of $[\bar{1}10]$ -oriented dimers in 2×4 surface reconstructions is in accordance with MOVPE-grown AlInP surfaces in N_2 atmosphere.^[13] Heterodimer structures featuring either In–P or Al–P dimers in the topmost layer occur for cation-rich preparation conditions. They differ from the mixed-dimer structure known from InP(001) by the staggered arrangement

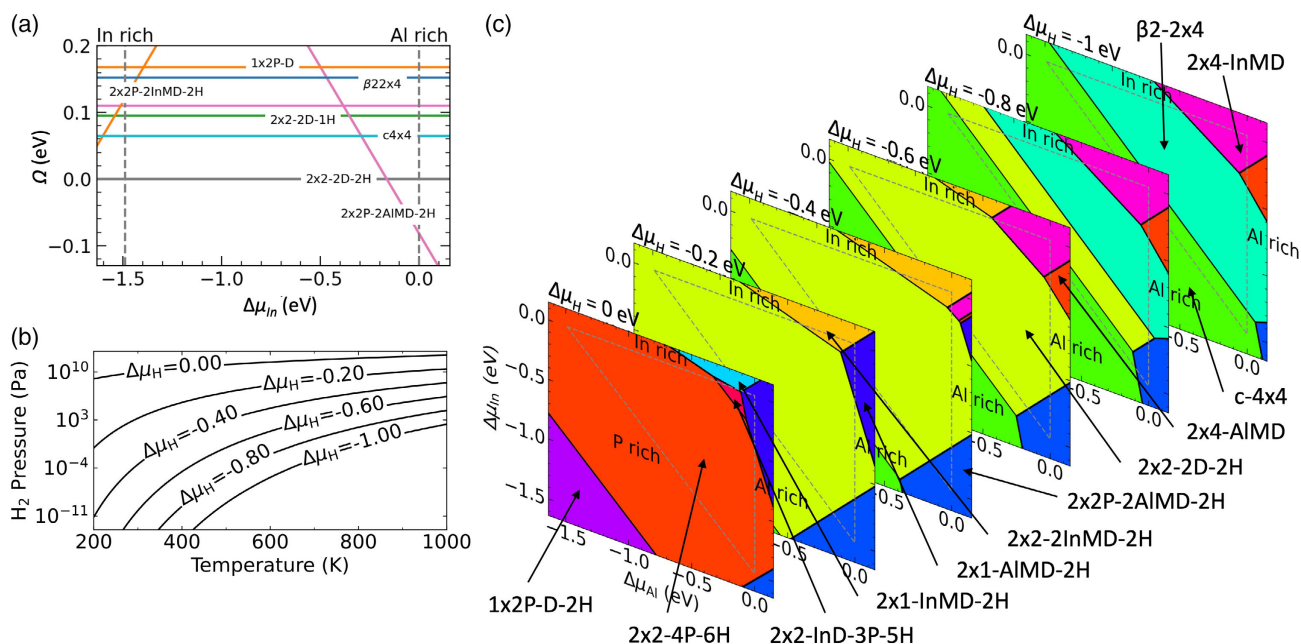


Figure 1. a) $\text{Al}_{0.5}\text{In}_{0.5}\text{P}(001)$ surface phase diagram calculated assuming P-rich surfaces and $\Delta\mu_{\text{H}} = -0.6$ eV, that is, preparation conditions typical for vapor-phase epitaxy. Energies are given relative to the 2×2 -2D-2H surface. b) Dependence of the hydrogen chemical potential on temperature and partial pressure according to Equation (4). c) Complete surface phase diagram depending on the Al, In, and H chemical potentials. The thermodynamically allowed range of the chemical potentials according to Equation (2) and (3) is indicated by dashed lines. See Figure 2 for the notation of surface structures.

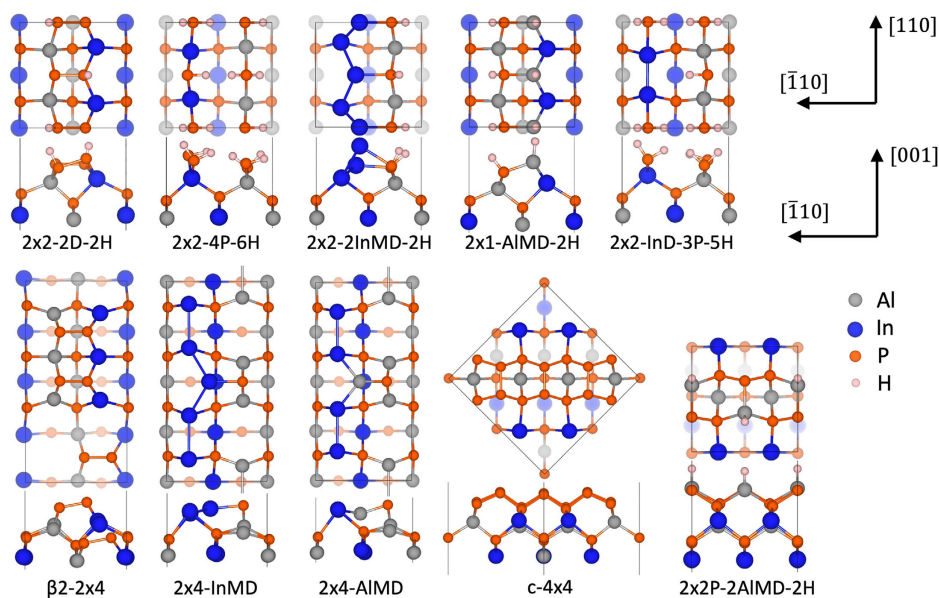


Figure 2. Top and side views of stable relaxed clean as well as hydrogenated $\text{Al}_{0.5}\text{In}_{0.5}\text{P}(001)$ surface structures identified in the present work.

of the second-layer cation dimers, due to the size mismatch between Al and In.

For a broad range of intermediate values of the hydrogen chemical potential, $\Delta\mu_{\text{H}} = -0.2$ eV \dots -0.8 eV, the 2D-2H surface is found to be stable; see Figure 1a. It corresponds to a 2×2 -reconstructed surface formed by P dimers; see Figure 2. Hydrogen is adsorbed in an alternating sequence

on these buckled P dimers. Similar structures were observed for the (001) surface of InP, GaP, and $\text{In}_x\text{Ga}_{1-x}\text{P}$ prepared by gas-phase epitaxy.^[20,21,29]

The P dimers of the 2×2 -2D-2H surface break up at extremely H-rich conditions, $\Delta\mu_{\text{H}} = 0$ eV. In this case, the surface P atoms are alternately decorated by one and two hydrogens, forming the 2×2 -4P-6H structure. The hydrogen-

covered surface P atoms are replaced by H-decorated In–P and Al–P heterodimers, if the surface is prepared in hydrogen and cation-rich conditions.

Zunger et al.^[30] suggested that the creation of subsurface selectivity for occupation by a small cation under the strained anion dimer rows and occupation by a large cation underneath the opening between dimer rows is the main thermodynamic driving force for CuPt ordering in GaInP alloys. The present calculations support this picture for AlInP. All stable P dimer structures identified here are characterized by P dimers that form above Al, while In occupies the corresponding subsurface positions between the P dimer rows; see Figure 2. No such correlation is found for the heterodimer structures. Mixed anion–cation dimers form on top of In, for example, in the 2×2 -2InMD-2H structure, as well as above Al, for example, in the 2×1 -AlMD-2H structure. This agrees with the observation that the degree of atomic ordering of MOVPE-grown AlInP depends sensitively on the preparation conditions.^[13]

3.2. Experiment

In order to compare the theoretical calculations with the surface reconstruction of $\text{Al}_{0.5}\text{In}_{0.5}\text{P}(001)$ obtained experimentally, thin $\text{Al}_{0.52}\text{In}_{0.48}\text{P}(001)$ layers were prepared in a horizontal MOVPE reactor using H_2 carrier gas at 100 mbar. The AlInP(001) epilayers were grown on GaInP(001) buffer layers on *n*-GaAs(001) substrate with 0.1° miscut toward the [111] direction. After deoxidation of GaAs(001) substrate under tertiarybutylarsine at 620°C (surface temperature), 100 nm GaAs(001) and 100 nm GaInP(001) buffer layers were grown. Tertiarybutylphosphine (TBP), trimethylindium (TMIn), trimethylgallium (TMGa), and trimethylaluminium (TMAI) were used as precursors. The epitaxially grown layers were doped n-type ($\approx 1 \times 10^{17} \text{ cm}^{-3}$) using ditertiarybutyl silane (DTBSi). The $\text{Al}_{0.52}\text{In}_{0.48}\text{P}(001)$ layer was grown at 100 mbar with a V/III ratio of 60 at 600°C . To compensate the desorption of P from the AlInP(001) surface during cooling, the TBP precursor was kept open until reaching 300°C . Subsequently, the TBP precursor was switched off and the sample was annealed for 10 min at 310°C to remove the excess of P and TBP precursor residuals from the surface. Lattice matching of the GaInP(100) and AlInP(001) layers to the substrate was confirmed ex situ by X-ray diffraction (XRD) in reference samples. To investigate the surface reconstruction and chemical composition of the as-prepared AlInP(001) surfaces, selected samples were transferred from the MOVPE reactor in ultrahigh vacuum (UHV) via a dedicated UHV shuttle^[31] for LEED (SPECS ErLEED 100-A) and XPS (SPECS Focus 500/Phoibos 150/1D-DLD-43-100, monochromated Al-K α , 1486.74 eV).

The preparation conditions (temperature and partial pressure) described above correspond to a H chemical potential of about -0.6 eV . For this chemical potential, the 2×2 -2D-2H surface is by far the most dominant structure in the phase diagram; see Figure 1. Figure 3 shows an XPS survey scan (top) as well as the Al 2*p*, In 3*d*_{5/2}, and P 2*p* (bottom, from left to right) core-level photoemission lines of the 32 nm-thick AlInP(001) film. To increase the surface sensitivity of the measurement, the photoelectron take-off angle (with respect to the surface

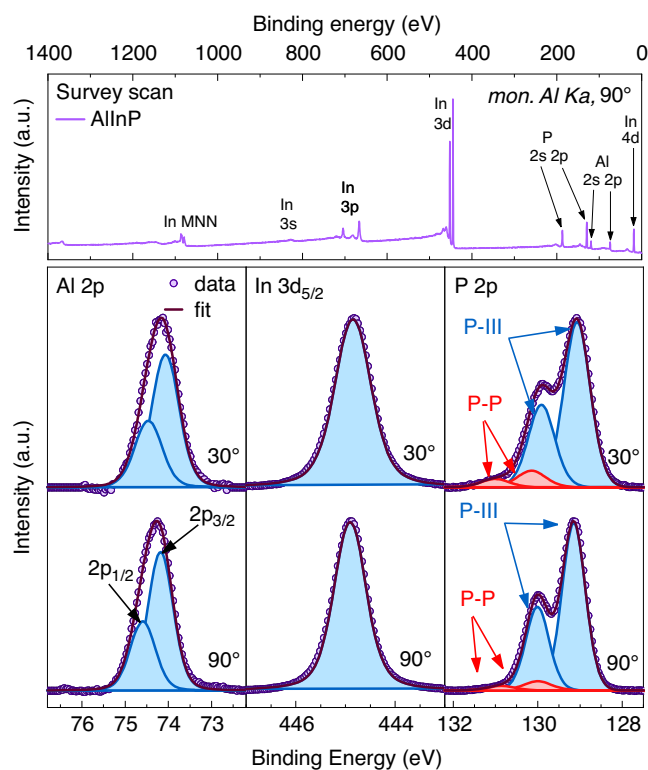


Figure 3. XPS survey spectrum of a 32 nm-thick $\text{Al}_{0.52}\text{In}_{0.48}\text{P}(001)$ layer (top) as well as the Al 2*p*, In 3*d*_{5/2}, and P 2*p* core-level photoemission lines measured at 30° (middle) and 90° (bottom) take-off angle (with respect to surface plane).

plane) was varied from 90° to 30° against normal emission (Figure 3, middle). The survey scan shows no oxygen or carbon on the sample. The fit of the XPS data shows that one component is sufficient to fit the Al 2*p*_{1/2}, Al 2*p*_{3/2}, and In 3*d*_{5/2} core-level peaks. The binding energy of metallic Al and In is at lower energy, at 72.75 and at 443.75 eV, respectively,^[32] and not seen in the measured data. For the P 2*p* core level, the presence of an extra component is obvious. The data are fitted with two spin-orbit pairs, with the same FWHM and peak ratio of 2:1 for each pair. The second, lower-intensity component (red line) is shifted toward higher binding energy, and its binding energy can be correlated with P dimers on the surface.^[32] The intensity ratio of the peak related to the P dimers increased at the more surface-sensitive measurement (P 2*p* core level, middle), which confirms a P-rich surface. Thus, the XPS measurements exclude cation-rich models and suggest P dimer structures such as the 2×2 -2D-2H or the β - 2×4 surface.

To further investigate the surface structure, LEED was applied. Figure 4 shows the LEED diffraction patterns recorded at 52 eV (left hand side) and 64 eV (right hand side). The slightly diffuse LEED pattern and spots with blurred contrast indicate a reduced atomic order of the surface. This could be due to surface defects, lack of short-range order in the surface reconstruction, for example, due to missing hydrogen passivation, or due to traces of contaminants such as oxygen. Aluminium containing surfaces are well known for their high affinity to oxygen incorporation.^[19] Nevertheless, the LEED patterns clearly exhibit first- and half-

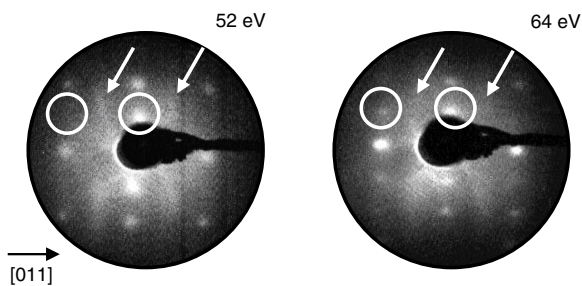


Figure 4. LEED pattern of the $\text{Al}_{0.52}\text{In}_{0.48}\text{P}(001)$ surface. See text.

order spots. In addition to the first-order spots, both diffraction patterns exhibit half-order spots indicating a 2×1 -like surface reconstruction (marked with white circles) and diffused streaks in $\times 2$ direction (indicated by white arrows). This LEED pattern is very similar to measurements on P-rich and partially hydrogen-covered $\text{InP}(001)$ and $\text{GaP}(001)$ surfaces: The adjacent rows of buckled P dimers stabilized by one hydrogen atom can be arranged in phase or out of phase.^[20,33,34] The in-phase arrangement results in a $p \times 2$ unit cell, while the out-of-phase arrangement corresponds to a $c \times 2$ unit cell. Scanning tunneling microscopy (STM) scans of such P-rich $\text{InP}(001)$ and $\text{GaP}(001)$ surfaces show that those two domains are randomly distributed.^[33,34] Their superposition leads to the 2×1 -like LEED pattern with characteristic streaks in the $\times 2$ half-order (see Figure 1 in the study by Kleinschmidt et al.^[34]). This excludes the $\beta 2 \times 4$ surfaces and is strong evidence that the surface prepared here corresponds to the $2 \times 2\text{-}2\text{D}\text{-}2\text{H}$ reconstruction predicted from ab initio thermodynamics.

3.3. Surface Electronic Properties

Binary III–V surface reconstructions can be understood in terms of a simple electron counting model (ECM):^[35] A surface structure satisfies this model if all cation dangling bonds are empty

and all anion dangling bonds are full, given the number of available electrons. This model may be extended to hydrogen-covered surfaces^[36] and is satisfied by the majority of the stable ternary surface structures identified here. In fact, the $2 \times 1\text{-AlMD}\text{-}2\text{H}$ structure is the only exception to the ECM. It is stable in a very narrow range of preparation conditions that are both cation and hydrogen rich.

The $2 \times 1\text{-AlMD}\text{-}2\text{H}$ structure is not only the only stable structure that does not comply with the ECM. It is also the only structure that gives rise to a metallic band structure; see Figure 5. It features 1D Al–In atomic wires along the $[110]$ direction, which are partially H decorated. The Al–In metal bonds result in a quasi-1D electron band, which disperses along the atomic wire direction and pins the Fermi energy at midgap position. Similar electronic properties are calculated for the $2 \times 2\text{-}2\text{InMD}\text{-}2\text{H}$ structure. Here, an In–In atomic wire extends along the $[110]$ direction and gives rise to two strongly dispersive electron bands. These two bands, one occupied and one empty, are separated by a small bandgap of about 0.2 eV and pin the Fermi energy at midgap position. However, these two structures are stable only in a very small window of preparation conditions, where the cation-rich surface is exposed to hydrogen.

The $\beta 2 \times 4$, the $2 \times 2\text{-}4\text{P}\text{-}6\text{H}$, and, in particular the $2 \times 2\text{-}2\text{D}\text{-}2\text{H}$ structures are far more prominent in the calculated surface phase diagram. They correspond to P-rich surfaces without hydrogen, in extremely hydrogen-rich, and at intermediate conditions, respectively. In case of the $2 \times 2\text{-}2\text{D}\text{-}2\text{H}$ structure, an occupied bound surface state is observed that extends slightly above the bulk valence band maximum (VBM), see Figure 5. This state is mainly related to the dangling bonds on the up atom of the phosphorus dimer. Exposing the P-rich $\text{AlInP}(001)$ surface to very hydrogen-rich conditions leads to the $2 \times 2\text{-}4\text{P}\text{-}6\text{H}$ structure and removes essentially all surface states from the band gap region. In fact, the only remaining surface state occurs at about 0.2 eV below the bulk VBM and corresponds to dangling bonds at under-coordinated surface P atoms. In case of the hydrogen-free $\beta 2 \times 4$ surface, an occupied surface state is observed at about

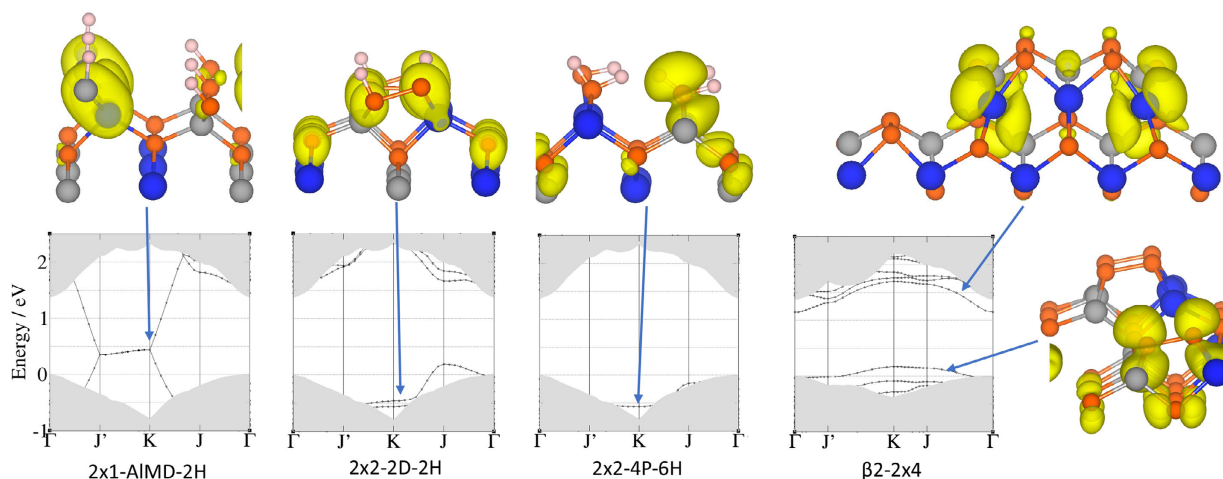


Figure 5. Band structures of the thermodynamically most relevant surface structures as well as of the $2 \times 1\text{-AlMD}\text{-}2\text{H}$ surface. Gray regions indicate the projected bulk band structure. Γ and Γ' are parallel to $\bar{\Gamma}10$ and $[110]$, respectively. The orbital character of state (at the K point) is indicated for prominent surface states. See Figure 2 for notation of atoms.

0.2 eV above the bulk VBM. This only weakly dispersive feature corresponds to an antibonding π^* combination of p_z orbitals localized at the third-layer P dimer. In addition, an empty surface state extends slightly into the region of the bulk bandgap. It is related to empty dangling bonds located at the threefold-coordinated second-layer cations. It is mainly In localized, but also has some Al contribution.

Generally, with the exception of the 2×1 -AlMD-2H and 2×2 -InMD-2H structures discussed above, it is found that all stable surfaces are characterized by occupied surface states close to the bulk VBM that are derived from surface anions or anion–cation bonds. The unoccupied surface states occur close to the bulk conduction band minimum and are cation related.

4. Conclusion

In summary, it is shown that the AlInP(001) surface produced in the MOVPE environment is composed of a complete layer of phosphorus dimers. Half of the P dangling bonds on the dimers are hydrogen saturated, and the other half are filled with lone pairs of electrons. These lone pairs form a bound surface state slightly above the valence band maximum. DFT calculations suggest the existence of further structures, depending on the surface preparation conditions. P-rich surfaces are characterized by P dimers, while Al–P and In–P heterodimers form for more cation-rich surface preparation conditions. Most stable surface structures obey the electron counting rule. Dimer-related surface states are found close to the bulk valence band maximum. Exposure of the surface to extreme hydrogen-rich conditions is predicted to quench the dimerization and remove all surface states from the region of the bulk bandgap. For cation- and hydrogen-rich preparation conditions, metal atomic wires may form on the surface. They give rise to quasi-1D surface bands that pin the Fermi energy in the midgap region.

Acknowledgements

Financial support by DFG (PAK981) is gratefully acknowledged. The authors thank the Paderborn Center for Parallel Computing (PC²) and the Höchstleistungs-Rechenzentrum Stuttgart (HLRS) for grants of high-performance computer time.

Open Access funding enabled and organized by Projekt DEAL.

Conflict of Interest

The authors declare no conflict of interest.

Data Availability Statement

The data that support the findings of this study are available from the corresponding author upon reasonable request.

Keywords

AlInP, density functional theory, electronic properties, surface structures, X-ray photoelectron spectroscopy

Received: July 11, 2022
Revised: July 29, 2022
Published online: August 19, 2022

- [1] McEvoy's Handbook of Photovoltaics: Fundamentals and Applications (Ed: S. A. Kalogirou), Academic Press, Cambridge MA 2017.
- [2] C.-W. Kim, G.-Y. Park, J.-C. Shin, H.-J. Kim, *Appl. Sci.* **2022**, *12*, 601.
- [3] D. L. Lepkowski, T. Kasher, J. T. Boyer, D. J. Chmielewski, T. J. Grassman, S. A. Ringel, *IEEE J. Photovoltaics* **2020**, *10*, 758.
- [4] K. Iwata, H. Asahi, T. Ogura, J. Sumino, S. Gonda, A. Ohki, Y. Kawaguchi, T. Matsuoka, in *Seventh Int. Conf. on Indium Phosphide and Related Materials*, Sapporo, Japan **1995**, pp. 183–186.
- [5] S. T. Murphy, A. Chroneos, C. Jiang, U. Schwingenschlögl, R. W. Grimes, *Phys. Rev. B* **2010**, *82*, 073201.
- [6] J. W. Nicklas, J. W. Wilkins, *Appl. Phys. Lett.* **2010**, *97*, 091902.
- [7] A. Abdollahi, M. M. Golzan, *J. Mater. Sci.* **2016**, *51*, 7343.
- [8] D. A. Beaton, T. Christian, K. Alberi, A. Mascarenhas, K. Mukherjee, E. A. Fitzgerald, *J. Appl. Phys.* **2013**, *114*, 203504.
- [9] S.-H. Wei, A. Zunger, *Appl. Phys. Lett.* **1998**, *72*, 2011.
- [10] Y.-H. Li, A. Walsh, S. Chen, W.-J. Yin, J.-H. Yang, J. Li, J. L. F. Da Silva, X. G. Gong, S.-H. Wei, *Appl. Phys. Lett.* **2009**, *94*, 212109.
- [11] L. Meier, C. Braun, T. Hannappel, W. G. Schmidt, *Phys. Status Solidi B* **2021**, *258*, 2000463.
- [12] L. Meier, W. G. Schmidt, *Phys. Status Solidi B* **2022**, *259*, 2100462.
- [13] Z. Jinghua, T. Xiaohong, T. Jinghua, *CrystEngComm* **2009**, *11*, 1068.
- [14] W. Yuan, D. C. Hall, *J. Appl. Phys.* **2013**, *113*, 103515.
- [15] S. B. Zhang, S. Froyen, A. Zunger, *Appl. Phys. Lett.* **1995**, *67*, 3141.
- [16] S. Froyen, A. Zunger, *Phys. Rev. Lett.* **1991**, *66*, 2132.
- [17] R. M. France, W. E. McMahon, J. Kang, M. A. Steiner, J. F. Geisz, *J. Appl. Phys.* **2014**, *115*, 053502.
- [18] G. Martín, C. Coll, L. López-Conesa, J. M. Rebled, E. Barrigón, I. García, I. Rey-Stolle, C. Algora, A. Cornet, S. Estradé, F. Peiró, *ACS Appl. Electron. Mater.* **2022**, *4*, 3478.
- [19] I. A. Ruiz Alvarado, M. Karmo, E. Runge, W. G. Schmidt, *ACS Omega* **2021**, *6*, 6297.
- [20] W. G. Schmidt, P. H. Hahn, F. Bechstedt, N. Esser, P. Vogt, A. Wange, W. Richter, *Phys. Rev. Lett.* **2003**, *90*, 126101.
- [21] P. H. Hahn, W. G. Schmidt, F. Bechstedt, O. Pulci, R. Del Sole, *Phys. Rev. B* **2003**, *68*, 033311.
- [22] W. G. Schmidt, *Appl. Phys. A* **2002**, *75*, 89.
- [23] G. Kresse, J. Furthmüller, *Comput. Mater. Sci.* **1996**, *6*, 15.
- [24] J. P. Perdew, K. Burke, M. Ernzerhof, *Phys. Rev. Lett.* **1996**, *77*, 3865.
- [25] P. E. Blöchl, *Phys. Rev. B* **1994**, *50*, 17953.
- [26] G. Kresse, D. Joubert, *Phys. Rev. B* **1999**, *59*, 1758.
- [27] S. Wippermann, W. G. Schmidt, *Phys. Rev. Lett.* **2010**, *105*, 126102.
- [28] W. G. Schmidt, *Appl. Phys. A* **1997**, *65*, 581.
- [29] S. F. Cheng, Y. Sun, D. C. Law, S. B. Visbeck, R. F. Hicks, *Surf. Sci.* **2006**, *600*, 2924.
- [30] J. E. Bernard, S. Froyen, A. Zunger, *Phys. Rev. B* **1991**, *44*, 11178.
- [31] T. Hannappel, S. Visbeck, L. Töben, F. Willig, *Rev. Sci. Instrum.* **2004**, *75*, 1297.
- [32] J. Moulder, J. Chastain, *Handbook of X-Ray Photoelectron Spectroscopy: A Reference Book of Standard Spectra For Identification and Interpretation of XPS Data*, Physical Electronics Division, Perkin-Elmer Corporation, Eden Prairie, Minnesota **1992**, ISBN 9780962702624.
- [33] L. Li, B.-K. Han, Q. Fu, R. F. Hicks, *Phys. Rev. Lett.* **1999**, *82*, 1879.
- [34] P. Kleinschmidt, H. Döscher, P. Vogt, T. Hannappel, *Phys. Rev. B* **2011**, *83*, 155316.
- [35] M. D. Pashley, *Phys. Rev. B* **1989**, *40*, 10481.
- [36] M. Karmo, I. A. Ruiz Alvarado, W. G. Schmidt, E. Runge, *ACS Omega* **2022**, *7*, 5064.